Aortic Remodeling is Modest and Sex-Independent in Mice When Hypertension is Superimposed on Aging

Bart SPRONCK[1,2,*], Jacopo FERRUZZI[1,*], Chiara BELLINI[3], Alexander W. CAULK[1], Sae-Il MURTADA[1], Jay D. HUMPHREY[1,4]

[1]Department of Biomedical Engineering
Yale University, New Haven, CT, USA

[2]Department of Biomedical Engineering
Maastricht University, Maastricht, The Netherlands

[3]Department of Bioengineering,
Northeastern University, Boston, MA, USA

[4]Vascular Biology and Therapeutics Program
Yale School of Medicine, New Haven, CT, USA

[*]These authors contributed equally

Address for Correspondence:
Bart Spronck, Ph.D.
Dept. of Biomedical Engineering
Yale University
55 Prospect St
New Haven, CT 06511
United States
Phone: +1 203 432 6678
E-mail: bart.spronck@yale.edu

Supplemental Methods

Induced Hypertension. To facilitate a consistent comparison with prior findings for healthy young (20 week) and naturally aged (100 week) wild-type (*Fbln5*$^{+/+}$) mice [S1] and similarly for young fibulin-5 null (*Fbln5*$^{-/-}$) mice [S2], we generated *Fbln5*$^{+/+}$ and *Fbln5*$^{-/-}$ mice of both sexes by breeding *Fbln5*$^{+/-}$ mice. After reaching adulthood, chronic hypertension was induced either by providing a high salt diet (8% NaCl chow; Harlan Teklad, Madison, WI) for 13 weeks with ad libitum drinking water containing an inhibitor of endothelial nitric oxide synthase (3 g/L of N(G)-Nitro-L-arginine methyl ester, or L-NAME; Sigma-Aldrich, St. Louis, MO) or by implanting subcutaneously an osmotic mini-pump that delivered angiotensin II (AngII) continuously for 14 days at 490 ng/kg/min. Inhaled isoflurane induced (3%) and maintained (1.5%) anesthesia during pump implantation and subcutaneous buprenorphine (0.1 mg/kg) provided analgesia immediately before the first surgical incision and post-operatively. Both Salt+L-NAME and AngII infusion increased blood pressure as measured with a standard tail cuff method just prior to euthanasia via an intraperitoneal injection of Beuthanasia-D (150 mg/kg; Merck, Whitehouse Station, NJ), and isolation of the proximal descending thoracic aorta (DTA) and infrarenal abdominal aorta (IAA) for *in vitro* mechanical testing. All animal protocols conformed to the current National Institutes of Health guidelines and were approved by the Yale University Institutional Animal Care and Use Committee.

Biomechanical Phenotyping. Because central arteries experience biaxial wall stresses throughout each cardiac cycle, and to ensure consistency with our prior studies [S1-4], we employed a standardized biaxial testing protocol. Briefly, excised vessels were cleaned of loose perivascular tissue, cannulated on custom glass micro-pipets, and placed within a temperature- and pH-controlled biaxial testing system [S2,5]. Vessels were stretched axially to their estimated *in vivo* length, at which pressurization from 60-140 mmHg changes the measured axial force minimally [S6,7], then equilibrated mechanically via cyclic pressurization from 80-120 mmHg for 15 minutes; subsequent preconditioning consisted of four distension cycles from 10-140 mmHg at the same stretch. Each vessel was then subjected to a series of seven biaxial loading protocols: cyclic pressurization from 10-140 mmHg while the vessel was held isometrically at a fixed axial stretch equal to 95%, 100%, or 105% of the *in vivo* value (which provided additional information to ensure robust estimation of the constitutive parameters as described below), then cyclic axial loading while the vessel was held isobarically at 10, 60, 100, or 140 mmHg. Axial loading was performed from 0 mN up to a force equal to the maximum value measured during pressurization at 105% of the *in vivo* axial stretch. All testing was conducted with the vessel immersed in a buffered Hank's solution at room temperature, which maintains a near passive behavior. Further details can be found elsewhere [S2].

Data Analysis. Similarly, we used prior methods to reduce the mechanical data and compute key metrics of interest, including biaxial (circumferential and axial) wall stress and material stiffness as well as elastic energy storage [S2,5]. Briefly, because residual stresses homogenize the transmural distribution of wall stress and because radial stress tends to be an order of magnitude less than the in-plane components, we calculated mean values of in-plane Cauchy wall stress as a function of mean values of in-plane wall stretch, namely, $\sigma_\theta = \hat{\sigma}_\theta(\lambda_\theta, \lambda_z)$ and $\sigma_z = \hat{\sigma}_z(\lambda_\theta, \lambda_z)$, where (θ, z) denote circumferential and axial. Specifically,

$$\sigma_\theta = \frac{Pa}{h} \, , \qquad \sigma_z = \frac{f + \pi a^2 P}{\pi h (2a + h)} \, ,$$

where P is the distending pressure and f the transducer-measured axial force, with a and h the inner radius and wall thickness, both computed from on-line measurements of outer diameter as well as wall thickness in the unloaded state while assuming incompressibility. We used an independently validated [S8] four-fiber strain energy density function W to describe simultaneously the pressure-diameter and axial force-stretch data. Specifically, nonlinear regression revealed best-fit values of the material parameters in W that minimized differences between computed and measured pressures and axial forces from unloading responses during the last cycle of each of the seven testing protocols [S2,4], with

$$W\left(\mathbf{C}, \mathbf{M}^i\right) = \frac{c}{2}\left(tr\mathbf{C} - 3\right) + \sum_{i=1}^{4} \frac{c_1^i}{4c_2^i}\left\{\exp\left[c_2^i\left(\mathbf{M}^i \cdot \mathbf{C}\mathbf{M}^i - 1\right)^2\right] - 1\right\},$$

where $\mathbf{C} = \mathbf{F}^T\mathbf{F}$ is the right Cauchy-Green tensor, with $\mathbf{F} = \mathrm{diag}[\lambda_r, \lambda_\theta, \lambda_z]$ inferred from measured changes in diameter and length with $\det\mathbf{F} = 1$. $\mathbf{M}^i = \left[0, \ \sin\alpha_0^i, \ \cos\alpha_0^i\right]$ defined the direction of the ith family of fibers in a traction-free reference configuration. We included contributions of axial ($\alpha_0^1 = 0$), circumferential ($\alpha_0^2 = \pi/2$), and two symmetric diagonal families of fibers ($\alpha_0^{3,4} = \pm\alpha_0$) based on prior results from imaging and success in describing biaxial data from mice [S1-5,9]. The eight model parameters determined from nonlinear regression are: c, c_1^1, c_2^1, c_1^2, c_2^2, $c_1^{3,4}$, $c_2^{3,4}$, and α_0. Biaxial stress and material stiffness were computed via appropriate differentiation of W, then compared at physiologic pressures and *in vivo* axial stretches using one-way analysis of variance (ANOVA), with Tukey-Kramer post-hoc testing and $p < 0.05$ considered significant. Prior non-parametric bootstrapping studies revealed good fixed-point estimates of the material parameters using our constitutive relation and simultaneous fit to seven biaxial protocols [S10]. Normality of residuals was verified through residual plots. Values are listed as means ± standard errors unless noted otherwise.

Local Mechano-adaptation. Large arteries tend to develop so as to achieve and then maintain mechanical stresses near homeostatic targets [S11,12]. If we let $\gamma = P/P_o$ represent a fold-change in blood pressure P above normal (P_o) and similarly $\varepsilon = Q/Q_o$, where Q is the volumetric flowrate and Q_o its target value, then maintaining the mean circumferential wall stress ($\sigma_\theta = Pa/h$) and wall shear stress ($\tau_w = 4\mu Q/\pi a^3$, where μ is the viscosity of blood) near normal values requires that inner radius remodel as $a \rightarrow \varepsilon^{1/3} a_o$ and similarly for wall thickness $h \rightarrow \varepsilon^{1/3}\gamma h_o$ [S13]. Such geometric remodeling is said to be locally mechano-adaptive; if radius and thickness do not evolve to restore these stresses to normal, the response is mechanically maladaptive. In the case of constant cardiac output ($\varepsilon = 1$), mechano-adaptation requires that wall thickness change proportional to blood pressure ($h/h_o = \gamma = P/P_o$). Thus, we calculated and compared ratios of pressure, inner radius, and wall thickness for all aged and hypertensive groups with respect to their normotensive control groups.

Histology. Following mechanical testing, vessels were fixed overnight in the traction-free reference configuration using 4% formalin, then stored in 70% ethanol at 4°C until embedding in paraffin and sectioning at 5 μm. Verhoeff-Van Gieson (VVG) staining identified

3

elastic fibers (black); Masson's trichrome (MTC) identified fibrillar collagen (blue) and cell cytoplasm (red); Movat's (MOV) identified glycosaminoglycans (blue). Sections were imaged using an Olympus BX/51 microscope; further details can be found elsewhere [S1,4].

Supplemental References

S1.   Ferruzzi J, Madziva D, Caulk AW, Tellides G, Humphrey JD. Compromised mechanical homeostasis in arterial aging and associated cardiovascular consequences. *Biomech Model Mechanobiol* 2018; 17:1281-1295.

S2.   Ferruzzi J, Bersi MR, Uman S, Yanagisawa H, Humphrey JD. Decreased elastic energy storage, not increased material stiffness, characterizes central artery dysfunction in fibulin-5 deficiency independent of sex. *J Biomech Eng* 2015; 137:031007.

S3.   Bellini C, Wang S, Milewicz DM, Humphrey JD. Myh11(R247C/R247C) mutations increase thoracic aorta vulnerability to intramural damage despite a general biomechanical adaptivity. *J Biomech* 2015; 48:113-121.

S4.   Bersi MR, Khosravi R, Wujciak AJ, Harrison DG, Humphrey JD. Differential cell-matrix mechanoadaptations and inflammation drive regional propensities to aortic fibrosis, aneurysm or dissection in hypertension. *J R Soc Interface* 2017; 14.

S5.   Bersi MR, Bellini C, Wu J, Montaniel KRC, Harrison DG, Humphrey JD. Excessive adventitial remodeling leads to early aortic maladaptation in angiotensin-induced hypertension. *Hypertension* 2016; 67:890-896.

S6.   Weizsacker HW, Lambert H, Pascale K. Analysis of the passive mechanical properties of rat carotid arteries. *J Biomech* 1983; 16:703-715.

S7.   Humphrey JD, Eberth JF, Dye WW, Gleason RL. Fundamental role of axial stress in compensatory adaptations by arteries. *J Biomech* 2009; 42:1-8.

S8.   Schroeder F, Polzer S, Slazansky M, Man V, Skacel P. Predictive capabilities of various constitutive models for arterial tissue. *J Mech Behav Biomed Mater* 2018; 78:369-380.

S9.   Bellini C, Bersi MR, Caulk AW, Ferruzzi J, Milewicz DM, Ramirez F, et al. Comparison of 10 murine models reveals a distinct biomechanical phenotype in thoracic aortic aneurysms. *J R Soc Interface* 2017; 14.

S10.   Ferruzzi J, Bersi MR, Humphrey JD. Biomechanical phenotyping of central arteries in health and disease: advantages of and methods for murine models. *Ann Biomed Eng* 2013; 41:1311-1330.

S11.   Dajnowiec D, Langille BL. Arterial adaptations to chronic changes in haemodynamic function: coupling vasomotor tone to structural remodelling. *Clin Sci (Lond)* 2007; 113:15-23.

S12.   Baeyens N, Nicoli S, Coon BG, Ross TD, Van den Dries K, Han J, et al. Vascular remodeling is governed by a VEGFR3-dependent fluid shear stress set point. *Elife* 2015; 4:e04645.

S13.   Humphrey JD. Mechanisms of arterial remodeling in hypertension: coupled roles of wall shear and intramural stress. *Hypertension* 2008; 52:195-200.

S14.   Jiao Y, Li G, Korneva A, Caulk AW, Qin L, Bersi MR, et al. Deficient circumferential growth is the primary determinant of aortic obstruction attributable to partial elastin deficiency. *Arterioscler Thromb Vasc Biol* 2017; 37:930-941.

S15.   Bellini C, Korneva A, Zilberberg L, Ramirez F, Rifkin DB, Humphrey JD. Differential ascending and descending aortic mechanics parallel aneurysmal propensity in a mouse model of Marfan syndrome. *J Biomech* 2016; 49:2383-2389.

S16.   Roccabianca S, Figueroa CA, Tellides G, Humphrey JD. Quantification of regional differences in aortic stiffness in the aging human. *J Mech Behav Biomed Mater* 2014; 29:618-634.

S17.   Garcia-Herrera CM, Celentano DJ, Cruchaga MA, Rojo FJ, Atienza JM, Guinea GV, Goicolea JM. Mechanical characterisation of the human thoracic descending aorta: experiments and modelling. *Comput Methods Biomech Biomed Engin* 2012; 15:185-193.

S18.   Labrosse MR, Beller CJ, Mesana T, Veinot JP. Mechanical behavior of human aortas: Experiments, material constants and 3-D finite element modeling including residual stress. *J Biomech* 2009; 42:996-1004.

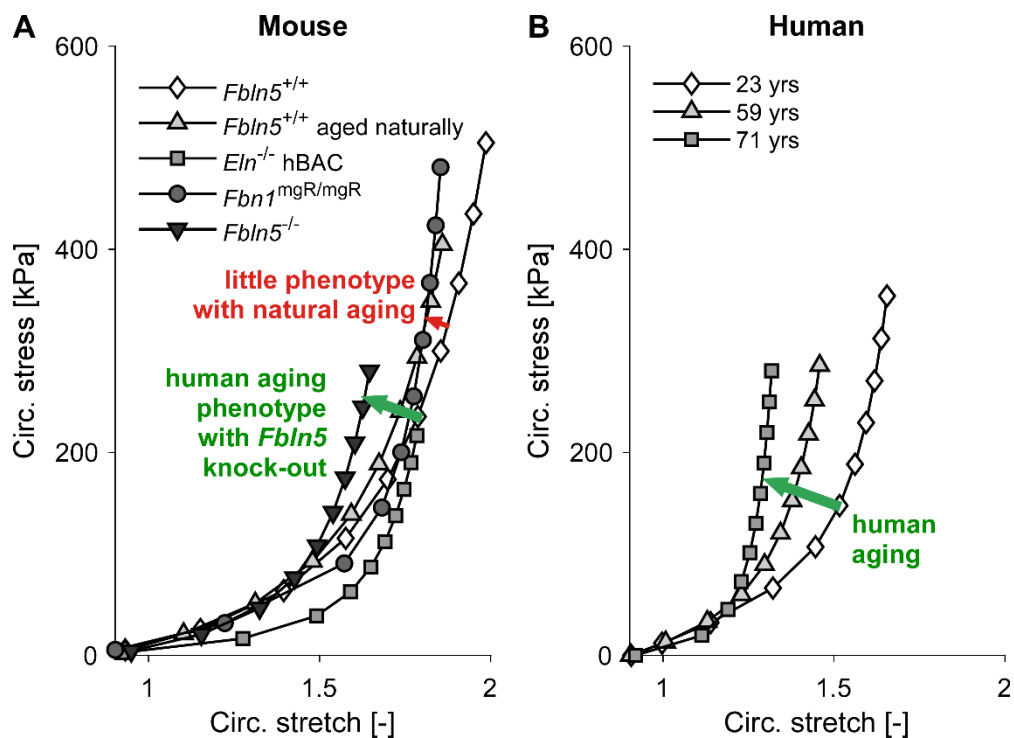**Figure S1**: Effects of natural aging on the mechanical properties of (**A**) murine (to 100 weeks) and (**B**) human (to 71 years) aging of the descending thoracic aorta (DTA), with additional murine data for three different cases of elastopathy: ~70% reduction in elastin ($Eln^{-/-}$ hBAC), ~75% reduction of fibrillin-1 ($Fbn1^{mgR/mgR}$), and complete loss of fibulin-5 ($Fbln5^{-/-}$). Whereas natural human aging is characterized by a marked leftward shift in the circumferential (circ.) stress-stretch relationship, due in part to a loss of elastic fiber integrity, this shift is not significant in natural murine aging. As it can be seen, however, several murine models of altered elastic fiber integrity phenocopy biomechanical aspects of human aging, especially mice that lack vascular fibulin-5. Murine data: $Fbln5^{+/+}$ and $Fbln5^{-/-}$, present study; $Fbln5^{+/+}$ aged, Ferruzzi et al. [S1]; murine elastin gene (*Eln*) knock-out incompletely rescued by human *ELN* in a bacterial artificial chromosome (hBAC), Jiao et al. [S14]; hypomorphic fibrillin-1 ($Fbn1^{mgR/mgR}$), Bellini et al. [S15]. Human data reported by Roccabianca et al. [S16] as re-derived from studies by García-Herrera et al. [S17] and Labrosse et al. [S18].
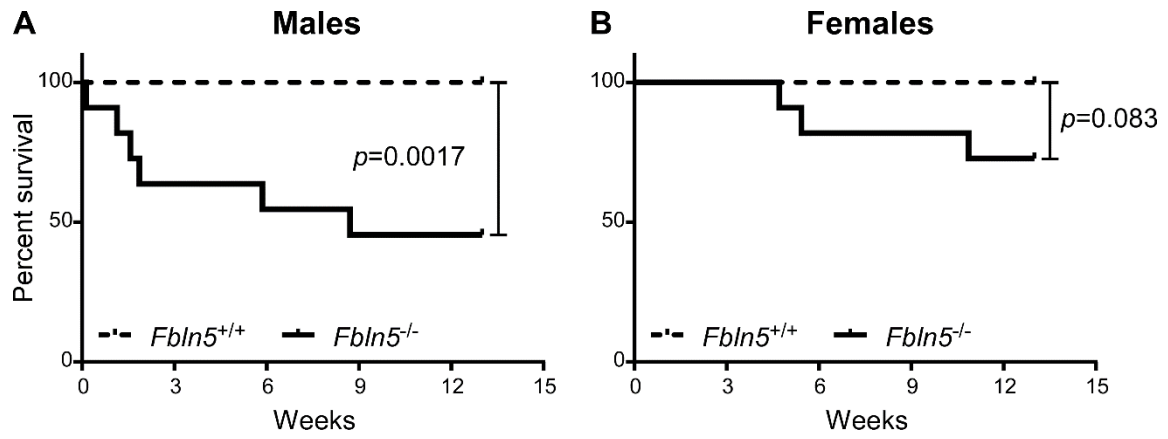
Figure S2: Salt+L-NAME treatment caused (**A**) a 55% mortality rate (6 out of 11) in the male fibulin-5 null mice but only (**B**) a 27% rate (3 out of 11) in the female fibulin-5 null mice on the same treatment. Kaplan-Meier curves, with *p* the *p*-value of Mantel-Cox tests.
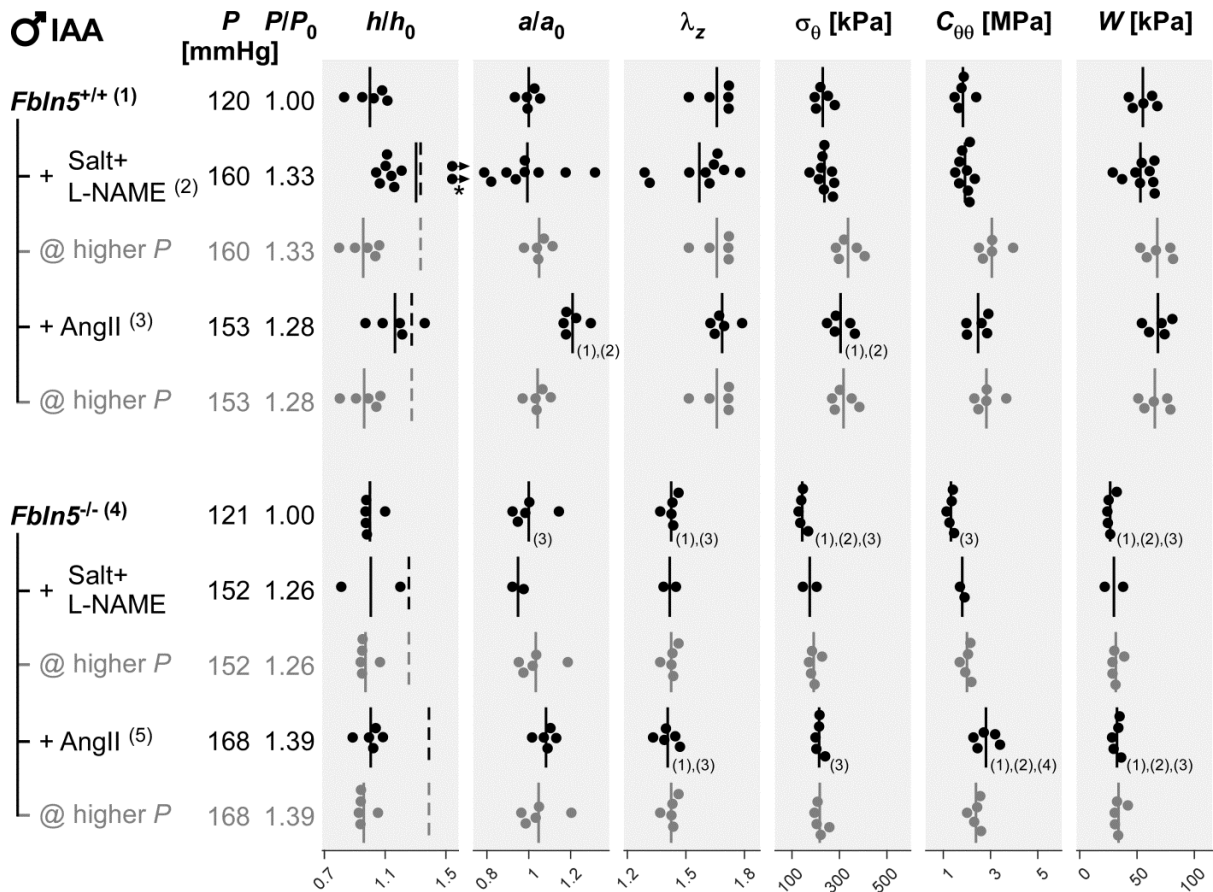
Figure S3: Select biomechanical metrics for the infrarenal abdominal aorta (IAA) from each animal in all six male study groups (black rows): $Fbln5^{+/+}$ (wild-type) mice without and with Salt+L-NAME or AngII induced hypertension and similarly for $Fbln5^{-/-}$ (knockout) mice. Results are for *in vivo* systolic pressures P (mmHg), pressure ratio $\gamma = P/P_o$, normalized wall thickness h/h_o, normalized luminal radius a/a_o, *in vivo* axial stretch λ_z and the mean circumferential Cauchy wall stress σ_θ (kPa), circumferential material stiffness $C_{\theta\theta}$ (MPa), and stored energy density W (kPa) calculated at the indicated pressure. A subscript "o" denotes original / homeostatic. Solid vertical lines indicate arithmetic means; dashed vertical lines represent a perfect mechano-adaptation given a constant cardiac output ($\varepsilon = 1$) but sustained increase in blood pressure ($h/h_0 = \gamma = P/P_o$), with under-adaptation indicated by a solid line to the left of the dashed line. Gray rows, labeled "@ higher P", show results for non-hypertensive groups but evaluated at pressures that match the Salt+L-NAME or AngII groups, which would not be adapted by definition. Numbers (1-5) in swarm plots indicate significant differences ($p < 0.05$, Bonferroni post-hoc test following three-way analysis of variance); between-sex comparisons – to data in Supplementary Fig. S4 – are indicated in **Fig. 1** with respect to the numbered group, 1 to 5; the $Fbln5^{-/-}$ + Salt+L-NAME group was excluded from statistics due to low sample size (n=2); statistical tests were also not performed for the "@ higher P" rows due to their direct (mathematical) relation to groups 1 and 4. An asterisk indicates h/h_0 values outside the plot range, which were not plotted to avoid compression of the other data points. AngII, angiotensin II. Group sizes (top to bottom): $Fbln5^{+/+}$: $n = 5, 9, 5, 5, 5$; $Fbln5^{-/-}$: $n = 5, 2, 5, 5, 5$.
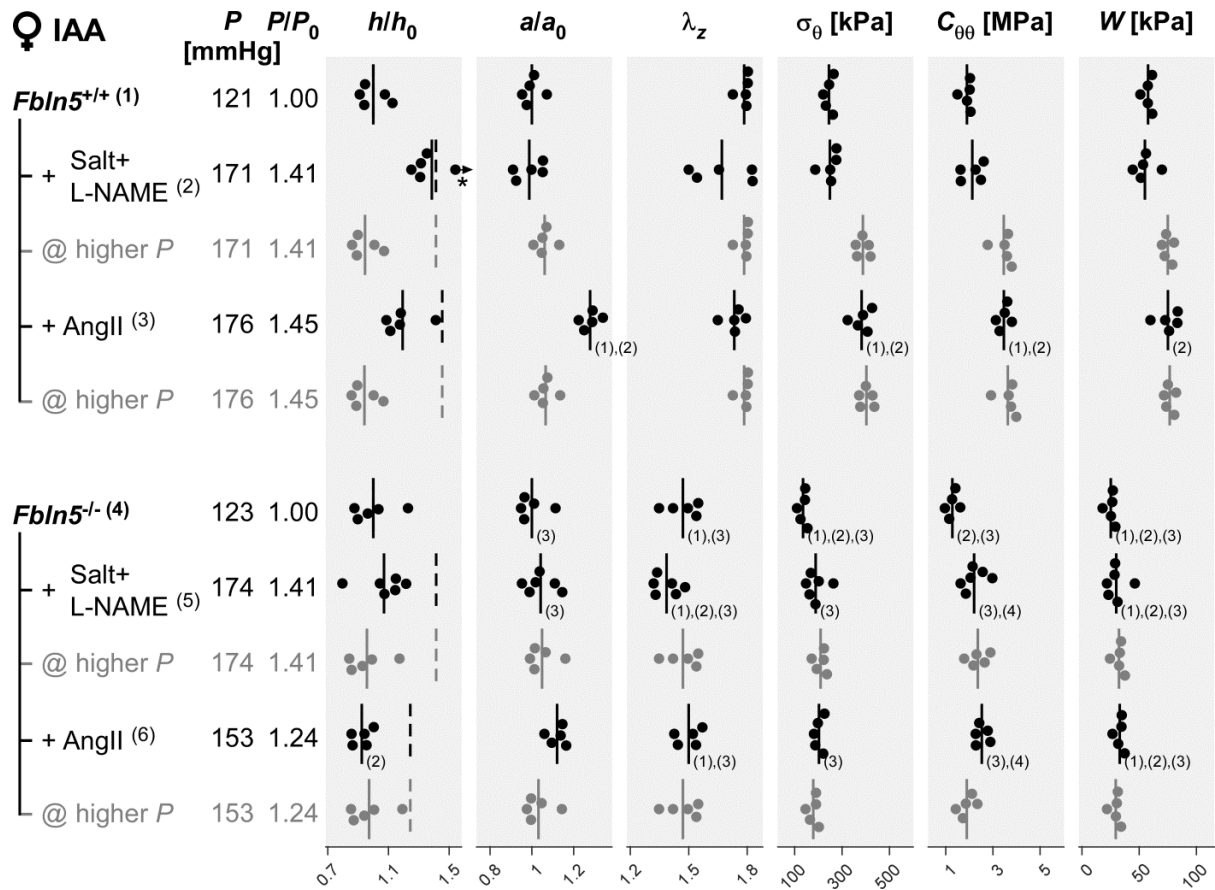
Figure S4: Similar to Fig. S3 except for the IAA from each animal in all six female study groups (1-6, black rows), including normotensive and induced hypertensive, as well as for normotensive vessels with metrics calculated for an acute increase in pressure (@ higher P) to the hypertensive levels. Numbers in swarm plots indicate significant differences ($p <$ 0.05, Bonferroni post-hoc test following three-way analysis of variance); between-sex comparisons – to data in Fig. S3 – are indicated in **Fig. 1**; statistical tests were not performed for the "@ higher P" rows. Group sizes (top to bottom): *Fbln5*^{+/+}: $n = 5, 5, 5, 5, 5$; *Fbln5*^{-/-}: $n = 5, 6, 5, 5, 5$.
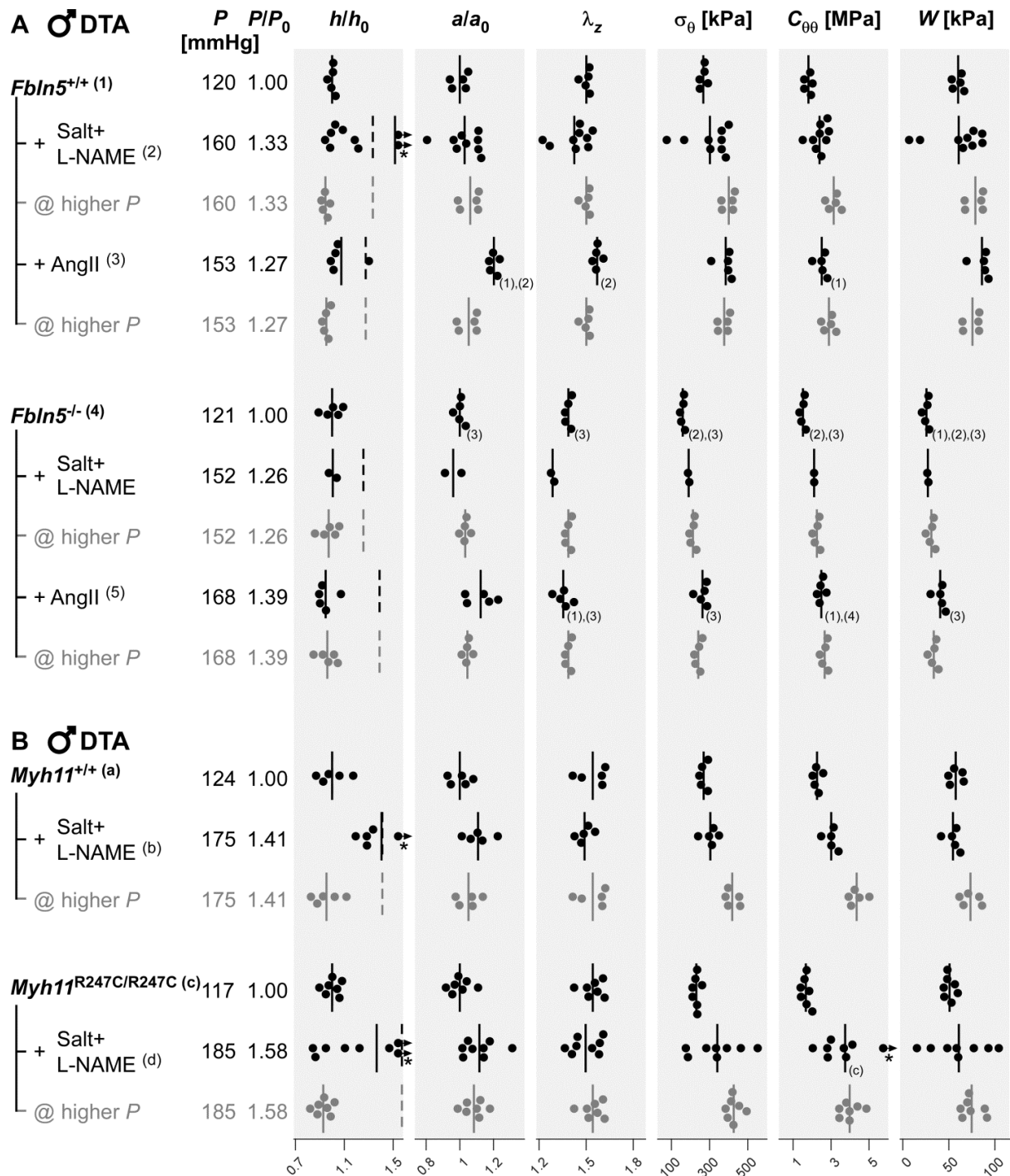
Figure S5: Biomechanical metrics for the descending thoracic aorta (DTA) from each animal in all six male study groups (**A**, black rows) as well as for re-calculated values for wild-type and knock-in *Myh11* mice that were reported previously (**B**, black rows) [S3]. Notation otherwise similar to that in Figs. S3 and S4, with numbers (panel **A**) and lowercase letters (panel **B**) in swarm plots indicating significant differences (**A**, $p < 0.05$, Bonferroni post-hoc test following three-way analysis of variance); between-sex comparisons – to data in Fig. S7 – are indicated in **Fig. 2**; **B**, $p < 0.05$, Bonferroni post-hoc test following two-way ANOVA); the *Fbln5*^{-/-} + Salt+L-NAME group was excluded from statistics due to low sample size (*n*=2); statistical tests were also not performed for the "@ higher *P*" rows. Asterisks indicate values of h/h_0 and $C_{\theta\theta}$ values outside the plot range (for *Fbln5*^{+/+} + Salt+L-NAME: $h/h_0 = 2.4$ and

3.8, for *Myh11*$^{+/+}$ + Salt+L-NAME: $h/h_0 = 1.9$, for *Myh11*$^{R247C/R247C}$ + Salt+L-NAME: $h/h_0 = 2.2$ and 2.3, $C_{\theta\theta} = 7.7$ MPa). These points were not plotted to avoid compression of the other data points. AngII, angiotensin II. Group sizes (top to bottom): *Fbln5*$^{+/+}$: $n = 5, 9, 5, 5, 5$; *Fbln5*$^{-/-}$: $n = 5, 2, 5, 5, 5$; *Myh11*$^{+/+}$: $n = 5, 5, 5$; *Myh11*$^{R247C/R247C}$: $n = 7, 8, 7$.
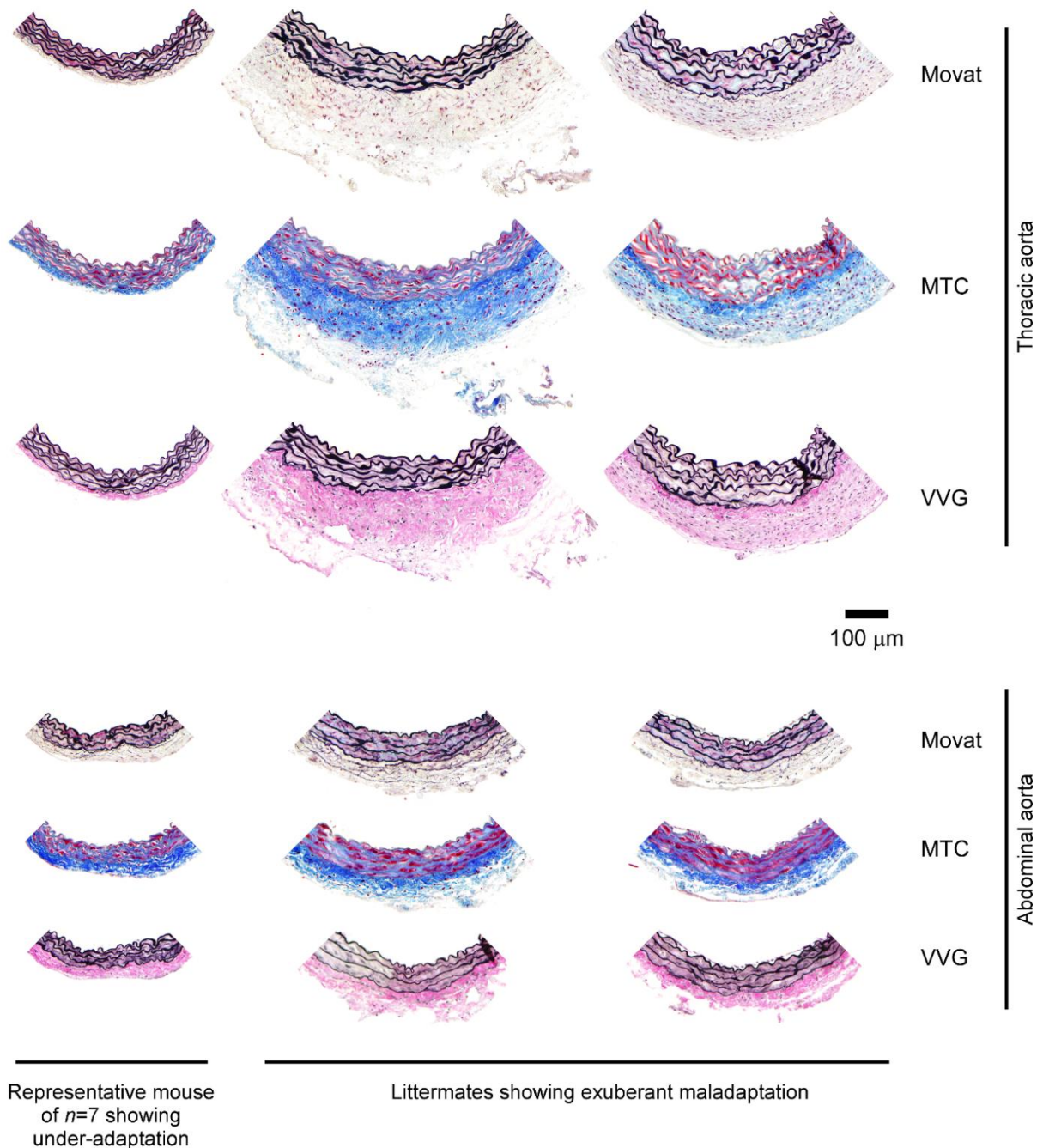
Figure S6: The 13-week treatment with Salt+L-NAME caused exuberant arterial remodeling of the descending thoracic aorta (top 3 rows) in two wild-type male littermates (middle and right columns) relative to most mice receiving the same treatment (left column). The infrarenal abdominal aortas (bottom 3 rows) showed the same trend, though less pronounced. Columns delineate histological sections from individual mice. Movat, VVG, and MTC: Movat's pentachrome, Verhoeff–Van Gieson, and Masson's trichrome stained histological images. Note the increased medial interlamellar spacing and glycosaminoglycan pooling in the middle and right columns, and the exuberant adventitial collagen deposition in these mice, especially in the adventitia of the DTA.
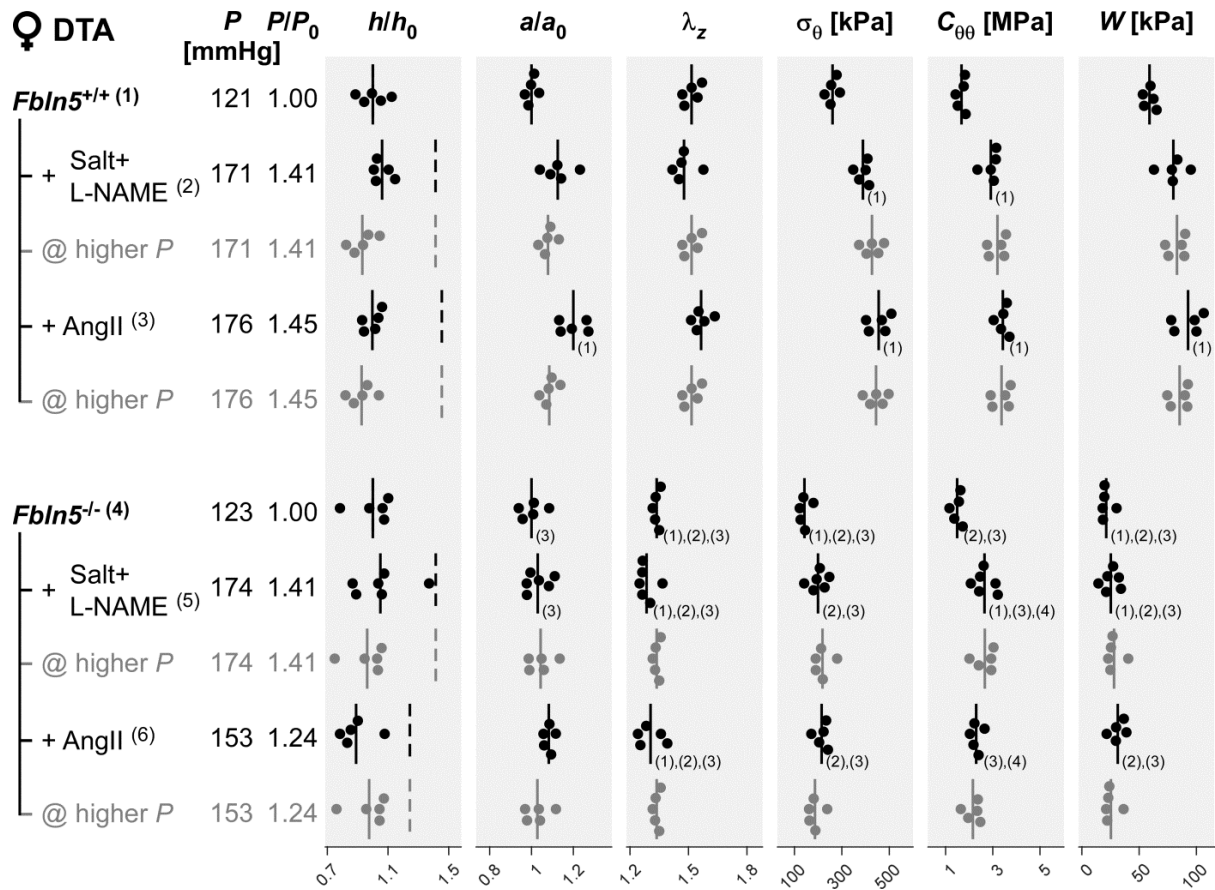
Figure S7: Biomechanical metrics for the DTA from each animal in all six female study groups (1-6, black rows). Notation similar to that in Fig. S3–S5. Numbers in swarm plots indicate significant differences ($p < 0.05$, Bonferroni post-hoc test following three-way analysis of variance); between-sex comparisons – to data in Fig. S5 – are indicated in **Fig. 2**; statistical tests were not performed for the "@ higher P" rows. AngII, angiotensin II. Group sizes (top to bottom): $Fbln5^{+/+}$: $n = 5, 5, 5, 5, 5$; $Fbln5^{-/-}$: $n = 5, 6, 5, 5, 5$.
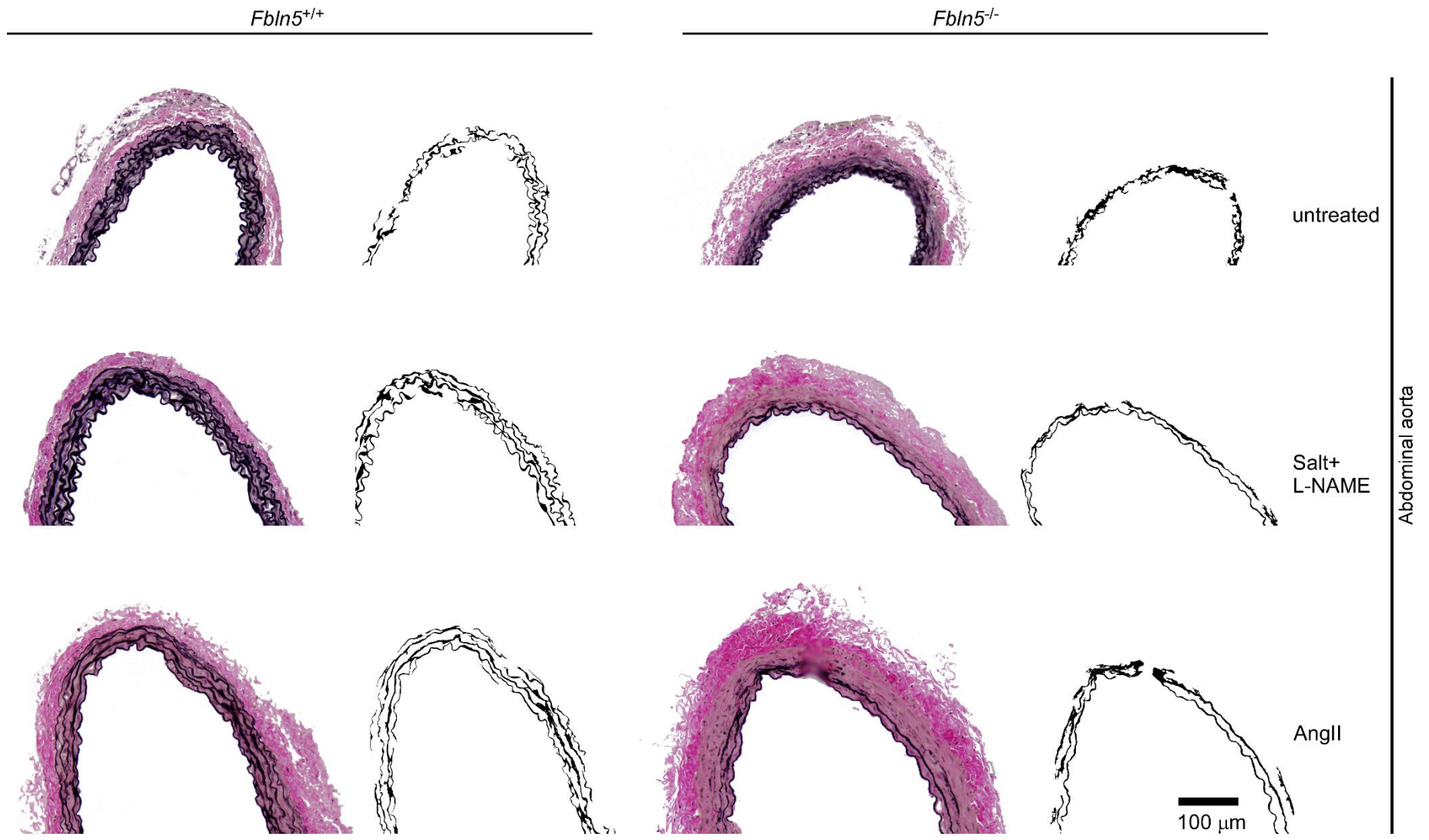
Figure S8: Representative Verhoeff–Van Gieson-stained male abdominal aortic sections. Note the incompletely formed elastic lamellae (stained in black) in the fibulin-5 (*Fbln5*) knock-out groups. For each group, an actual section is shown, along with a mask segmenting out the elastin alone by means of hue-saturation-lightness thresholding.

Figure S9: As Fig. S8, but for the male thoracic aorta.

Supplemental Tables

Table S1: Biomechanical metrics for the infrarenal abdominal aorta (IAA) of male mice.

|	Fbln5$^{+/+}$ (1)	Fbln5$^{+/+}$ Salt+L-NAME (2)	Fbln5$^{+/+}$ AngII (3)	Fbln5$^{-/-}$ (4)	Fbln5$^{-/-}$ Salt+L-NAME	Fbln5$^{-/-}$ AngII (5)	Fbln5$^{+/+}$ 100 wks (6)
	$n = 5$	$n = 9$	$n = 5$	$n = 5$	$n = 2$	$n = 5$	$n = 6$
Unloaded dimensions							
Wall Thickness, H (µm)	91 ± 3.4	106 ± 4.4	113 ± 7.6	100 ± 6.3	100 ± 14.7	98 ± 4.3	110 ± 2.0
Inner Diameter, $2A$ (µm)	406 ± 10	415 ± 33	466 ± 25	429 ± 21	400 ± 17	477 ± 6	403 ± 21
***In Vivo* (Loaded) Axial Stretch, λ_z**	1.66 ± 0.04	1.57 ± 0.06	1.69 ± 0.03	1.42 ± 0.02[1][3]	1.42 ± 0.03	1.41 ± 0.02[1][3]	1.55 ± 0.02
Dimensions at Diastolic Pressure P (mmHg)	$P = 84$	$P = 118$	$P = 110$	$P = 85$	$P = 110$	$P = 120$	$P = 64$
Wall Thickness, h (µm)	33 ± 1.7	42 ± 3.9	38 ± 2.2	47 ± 1.2[1]	47 ± 8.7	46 ± 1.6	51 ± 1.5[1]
Inner Diameter, $2a$ (µm)	804 ± 14.8	809 ± 47.5	978 ± 20.8[1][2]	738 ± 26.8[3]	711 ± 24.6	818 ± 12.0[3]	663 ± 22.7[2][3][5]
Dimensions at Systolic Pressure P (mmHg)	$P = 120$	$P = 160$	$P = 153$	$P = 121$	$P = 152$	$P = 168$	$P = 107$
Wall Thickness, h (µm)	31 ± 1.6	40 ± 3.8	36 ± 2.0	44 ± 1.1[1]	45 ± 8.6	45 ± 1.5[1]	44 ± 1.3[1]
Inner Diameter, $2a$ (µm)	866 ± 17.5	860 ± 48.6	1047 ± 20.8[1][2]	787 ± 30.4[3]	747 ± 21.2	852 ± 15.2[3]	780 ± 26.9[3]
Distensibility (1/MPa)	16.09 ± 1.05	11.51 ± 0.59[1]	12.33 ± 0.72[1]	13.81 ± 0.66	9.05 ± 1.16	6.36 ± 0.60[1][2][3][4]	30.77 ± 0.48[1][2][3][4][5]
Additional Metrics at Systolic Pressure							
Circumferential Stretch, λ_θ	1.80 ± 0.01	1.74 ± 0.04	1.88 ± 0.04	1.58 ± 0.05[1][3]	1.59 ± 0.04	1.56 ± 0.02[1][2][3]	1.61 ± 0.03[3]
Circumferential Cauchy Stress, σ_θ (kPa)	230 ± 16.0	237 ± 11.0	305 ± 21.8[1][2]	143 ± 6.9[1][2][3]	175 ± 29.0	214 ± 7.1[3][4]	126 ± 3.6[1][2][3][5]
Axial Cauchy Stress, σ_z (kPa)	231 ± 11.6	244 ± 19.5	261 ± 11.3	144 ± 5.6[1][2][3]	169 ± 42.0	165 ± 9.7[2][3]	151 ± 5.1[1][2][3]
Circumferential Linearized Material Stiffness, $\mathscr{C}_{\theta\theta\theta\theta}$ (MPa)	1.83 ± 0.15	1.92 ± 0.09	2.47 ± 0.20	1.32 ± 0.06[3]	1.80 ± 0.10	2.81 ± 0.21[1][2][4]	0.83 ± 0.02[1][2][3][5]
Axial Linearized Material Stiffness, $\mathscr{C}_{zzzz}$ (MPa)	2.92 ± 0.11	3.25 ± 0.30	3.80 ± 0.24	2.84 ± 0.21	3.59 ± 0.76	3.86 ± 0.24	1.81 ± 0.11[2][3][5]
Stored Strain Energy Density, W (kPa)	55 ± 4.8	53 ± 4.3	68 ± 4.8	27 ± 1.5[1][2][3]	30 ± 8.0	32 ± 1.5[1][2][3]	32 ± 1.0[1][2][3]
Dimensions at Fixed Pressure P (mmHg)	$P = 100$	$P = 100$	$P = 100$	$P = 100$	$P = 100$	$P = 100$	$P = 100$
Wall Thickness, h (µm)	32 ± 1.6	44 ± 4.0	39 ± 2.2	46 ± 1.2[1]	47 ± 8.8	47 ± 1.6[1]	45 ± 1.3
Inner Diameter, $2a$ (µm)	836 ± 16.2	777 ± 46.4	955 ± 20.9[2]	762 ± 28.5[3]	699 ± 25.7	796 ± 10.1[3]	767 ± 26.4[3]
Additional Metrics at Fixed Pressure	$P = 100$	$P = 100$	$P = 100$	$P = 100$	$P = 100$	$P = 100$	$P = 100$
Circumferential Stretch, λ_θ	1.74 ± 0.01	1.59 ± 0.03[1]	1.72 ± 0.03	1.53 ± 0.05[1][3]	1.50 ± 0.02	1.47 ± 0.02[1][3]	1.59 ± 0.03
Circumferential Cauchy Stress, σ_θ (kPa)	179 ± 12.5	121 ± 5.4[1]	167 ± 12.3[2]	111 ± 5.2[1][3]	101 ± 15.1	112 ± 3.6[1][3]	114 ± 3.2[1][3]
Axial Cauchy Stress, σ_z (kPa)	202 ± 11.1	176 ± 15.2	183 ± 7.8	124 ± 4.4[1]	122 ± 29.6	109 ± 6.1[1][2][3]	144 ± 5.1[1]
Circumferential Linearized Material Stiffness, $\mathscr{C}_{\theta\theta\theta\theta}$ (MPa)	1.31 ± 0.11	0.77 ± 0.03[1]	1.02 ± 0.09	0.92 ± 0.04[1]	0.81 ± 0.03	1.01 ± 0.09	0.72 ± 0.02[1]
Axial Linearized Material Stiffness, $\mathscr{C}_{zzzz}$ (MPa)	2.30 ± 0.08	1.92 ± 0.14	2.32 ± 0.16	2.34 ± 0.19	2.29 ± 0.37	2.09 ± 0.07	1.69 ± 0.10
Stored Strain Energy Density, W (kPa)	48 ± 4.3	37 ± 3.4	49 ± 3.3	23 ± 1.2[1][2][3]	22 ± 5.6	23 ± 0.7[1][2][3]	30 ± 0.9[1][3]

Values denote mean±standard error. Superscripted numbers in brackets indicate significant differences ($p < 0.05$, Bonferroni post-hoc test following 3-way analysis of variance (ANOVA)), and refer to group numbers. *Fbln5$^{-/-}$* + Salt+L-NAME group was not included in post-hoc testing due to low sample size ($n=2$).

Table S2: Biomechanical metrics for the infrarenal abdominal aorta (IAA) of female mice.

	$Fbln5^{+/+}$ (7)	$Fbln5^{+/+}$ Salt+L-NAME (8)	$Fbln5^{+/+}$ AngII (9)	$Fbln5^{-/-}$ (10)	$Fbln5^{-/-}$ Salt+L-NAME (11)	$Fbln5^{-/-}$ AngII (12)
	$n = 5$	$n = 5$	$n = 5$	$n = 5$	$n = 6$	$n = 5$
Unloaded dimensions						
Wall Thickness, H (μm)	82 ± 3.9[(2)(3)(6)]	98 ± 4.8	96 ± 2.9	94 ± 5.4	94 ± 3.7	92 ± 3.8
Inner Diameter, $2A$ (μm)	378 ± 14	398 ± 21	487 ± 11	402 ± 10	426 ± 15	439 ± 24
***In Vivo* (Loaded) Axial Stretch, λ_z**	1.78 ± 0.01[(2)(4)(5)(6)]	1.67 ± 0.07[(4)(5)]	1.73 ± 0.02[(4)(5)]	1.47 ± 0.04[(3)(7)(9)]	1.39 ± 0.03[(1)(2)(3)(7)(8)(9)]	1.50 ± 0.03[(7)(9)]
Dimensions at Diastolic Pressure P (mmHg)	$P = 86$	$P = 131$	$P = 125$	$P = 85$	$P = 133$	$P = 112$
Wall Thickness, h (μm)	28 ± 1.2[(2)(4)(5)(6)]	38 ± 2.2	33 ± 1.5[(4)(6)]	46 ± 3.0[(7)]	47 ± 2.7[(1)(7)(9)]	41 ± 1.2
Inner Diameter, $2a$ (μm)	732 ± 15.7[(3)]	739 ± 25.7[(3)]	949 ± 15.8[(2)(4)(6)(7)(8)]	655 ± 21.2[(2)(3)(5)(9)]	703 ± 20.7[(3)(9)]	755 ± 12.9[(3)(9)]
Dimensions at Systolic Pressure P (mmHg)	$P = 121$	$P = 171$	$P = 176$	$P = 123$	$P = 174$	$P = 153$
Wall Thickness, h (μm)	26 ± 1.1[(2)(4)(5)(6)]	36 ± 2.1	31 ± 1.5[(4)(5)(6)]	43 ± 2.7[(7)]	46 ± 2.6[(1)(7)(9)]	40 ± 1.2[(7)]
Inner Diameter, $2a$ (μm)	787 ± 15.8[(3)]	777 ± 23.9[(3)]	1006 ± 15.5[(2)(4)(6)(7)(8)]	699 ± 21.1[(1)(2)(3)(9)]	729 ± 20.9[(3)(9)]	784 ± 13.2[(3)(9)]
Distensibility (1/MPa)	15.98 ± 0.87[(2)(3)(5)(6)]	9.82 ± 1.02[(1)(4)(6)(7)]	8.91 ± 0.35[(1)(4)(6)(7)]	13.51 ± 0.65[(5)(6)(8)(9)]	6.57 ± 0.18[(1)(2)(3)(4)(6)(7)(10)]	6.96 ± 0.24[(1)(2)(3)(4)(6)(7)(10)]
Additional Metrics at Systolic Pressure						
Circumferential Stretch, λ_θ	1.77 ± 0.04[(5)]	1.64 ± 0.05[(3)]	1.78 ± 0.03[(4)(5)]	1.50 ± 0.06[(1)(2)(3)(7)(9)]	1.49 ± 0.02[(1)(2)(3)(7)(9)]	1.56 ± 0.05[(1)(2)(3)(7)(9)]
Circumferential Cauchy Stress, σ_θ (kPa)	245 ± 8.5[(4)(6)]	249 ± 16.4[(4)(6)]	383 ± 17.8[(1)(2)(3)(4)(5)(6)(7)(8)]	135 ± 8.0[(1)(2)(3)(5)(7)(8)(9)]	189 ± 16.8[(3)(9)]	203 ± 8.9[(3)(6)(9)]
Axial Cauchy Stress, σ_z (kPa)	274 ± 14.6[(4)(5)(6)]	255 ± 9.3[(4)(5)(6)]	319 ± 19.5[(1)(2)(4)(5)(6)]	149 ± 10.2[(1)(2)(3)(7)(8)(9)]	182 ± 10.1[(2)(3)(7)(8)(9)]	172 ± 9.3[(2)(3)(7)(8)(9)]
Circumferential Linearized Material Stiffness, $\mathscr{C}_{\theta\theta\theta\theta}$ (MPa)	1.90 ± 0.10[(5)(6)]	2.13 ± 0.21[(4)(6)]	3.46 ± 0.12[(1)(2)(3)(4)(6)(7)(8)]	1.28 ± 0.11[(3)(5)(8)(9)]	2.20 ± 0.20[(4)(6)(9)(10)]	2.53 ± 0.13[(4)(6)(9)(10)]
Axial Linearized Material Stiffness, $\mathscr{C}_{zzzz}$ (MPa)	3.23 ± 0.14	2.92 ± 0.49	5.38 ± 0.67[(1)(2)(4)(6)(7)(8)]	2.92 ± 0.27[(9)]	3.81 ± 0.23[(6)]	4.14 ± 0.41[(6)]
Stored Strain Energy Density, W (kPa)	58 ± 1.9[(4)(5)(6)]	55 ± 4.2[(4)(5)(6)]	75 ± 4.4[(1)(2)(4)(5)(6)(8)]	25 ± 1.9[(1)(2)(3)(7)(8)(9)]	30 ± 3.6[(1)(2)(3)(7)(8)(9)]	33 ± 1.8[(1)(2)(3)(7)(8)(9)]
Dimensions at Fixed Pressure P (mmHg)	$P = 100$	$P = 100$	$P = 100$	$P = 100$	$P = 100$	$P = 100$
Wall Thickness, h (μm)	27 ± 1.2[(2)(4)(5)(6)]	40 ± 2.3	34 ± 1.5	44 ± 2.8[(7)]	49 ± 2.8[(1)(7)(9)]	42 ± 1.3[(7)]
Inner Diameter, $2a$ (μm)	757 ± 15.8[(3)]	695 ± 27.5[(3)]	904 ± 16.1[(8)]	676 ± 21.1[(1)(3)(9)]	670 ± 20.1[(1)(3)(9)]	743 ± 12.8[(3)(9)]
Additional Metrics at Fixed Pressure	$P = 100$	$P = 100$	$P = 100$	$P = 100$	$P = 100$	$P = 100$
Circumferential Stretch, λ_θ	1.71 ± 0.03[(5)]	1.48 ± 0.04[(1)(3)(7)]	1.61 ± 0.03	1.45 ± 0.06[(1)(3)(7)]	1.38 ± 0.02[(1)(2)(3)(6)(7)(9)]	1.48 ± 0.05[(1)(3)(7)]
Circumferential Cauchy Stress, σ_θ (kPa)	188 ± 6.8[(2)(4)(5)(6)]	117 ± 8.6[(1)(3)(7)]	177 ± 7.5[(2)(4)(5)(6)(8)]	103 ± 6.3[(1)(3)(7)(9)]	93 ± 8.2[(1)(3)(7)(9)]	120 ± 5.3[(1)(3)(7)(9)]
Axial Cauchy Stress, σ_z (kPa)	240 ± 13.9[(2)(4)(5)(6)]	190 ± 11.0[(4)(5)]	199 ± 13.7[(4)(5)]	126 ± 8.8[(1)(7)(8)(9)]	127 ± 8.5[(1)(2)(3)(7)(8)(9)]	116 ± 7.1[(1)(2)(3)(7)(8)(9)]
Circumferential Linearized Material Stiffness, $\mathscr{C}_{\theta\theta\theta\theta}$ (MPa)	1.35 ± 0.08[(2)(4)(6)]	0.77 ± 0.08[(1)(7)]	1.15 ± 0.04[(2)(6)(8)]	0.87 ± 0.08[(1)(7)]	0.73 ± 0.05[(1)(7)(9)]	1.12 ± 0.06[(2)(6)(8)(11)]
Axial Linearized Material Stiffness, $\mathscr{C}_{zzzz}$ (MPa)	2.64 ± 0.10[(6)]	1.89 ± 0.16	2.94 ± 0.39[(2)(6)(8)]	2.34 ± 0.20	2.38 ± 0.15	2.28 ± 0.20
Stored Strain Energy Density, W (kPa)	50 ± 1.9[(2)(4)(5)(6)]	37 ± 2.7[(4)(5)]	49 ± 2.6[(4)(5)(6)]	22 ± 1.8[(1)(2)(3)(7)(8)(9)]	20 ± 2.6[(1)(2)(3)(7)(8)(9)]	25 ± 1.5[(1)(3)(7)(9)]

Values denote mean±standard error. Superscripted numbers in brackets indicate significant differences ($p < 0.05$, Bonferroni post-hoc test following 3-way analysis of variance (ANOVA)), and refer to group numbers; groups (1) to (6) are in Supplementary Table S1.

Table S3: Biomechanical metrics for the descending thoracic aorta (DTA) of male mice.

	$Fbln5^{+/+}$ (1)	$Fbln5^{+/+}$ Salt+L-NAME (2)	$Fbln5^{+/+}$ AngII (3)	$Fbln5^{-/-}$ (4)	$Fbln5^{-/-}$ Salt+L-NAME	$Fbln5^{-/-}$ AngII (5)	$Fbln5^{+/+}$ 100 wks (6)	$Myh11^{+/+}$ (a)	$Myh11^{+/+}$ Salt+L-NAME (b)	$Myh11^{R247C/R247C}$ (c)	$Myh11^{R247C/R247C}$ Salt+L-NAME (d)
	$n = 5$	$n = 9$	$n = 5$	$n = 5$	$n = 2$	$n = 5$	$n = 5$	$n = 5$	$n = 5$	$n = 7$	$n = 8$
Unloaded dimensions											
Wall Thickness, H (μm)	105 ± 2.5	128 ± 11.9	128 ± 5.7	116 ± 2.8	116 ± 4.7	112 ± 1.7	112 ± 2.4	98 ± 3.7	142 ± 13.9	106 ± 3.4	141 ± 14.8
Inner Diameter, $2A$ (μm)	618 ± 22	681 ± 48	669 ± 13	598 ± 20	524 ± 17	647 ± 35	660 ± 15	806 ± 24	805 ± 20	767 ± 11	806 ± 51
***In Vivo* (Loaded) Axial Stretch, λ_z**	1.50 ± 0.01	1.42 ± 0.04	1.57 ± 0.01[2]	1.39 ± 0.01[3]	1.29 ± 0.01	1.35 ± 0.02[1,3]	1.38 ± 0.03[3]	1.54 ± 0.04	1.49 ± 0.02	1.54 ± 0.03	1.50 ± 0.03
Dimensions at Diastolic Pressure P (mmHg)	$P = 84$	$P = 118$	$P = 110$	$P = 85$	$P = 110$	$P = 120$	$P = 64$	$P = 91$	$P = 127$	$P = 82$	$P = 141$
Wall Thickness, h (μm)	42 ± 0.5	61 ± 12.4	45 ± 2.4	57 ± 1.9	56 ± 1.9	54 ± 1.7	57 ± 1.5	44 ± 2.3	61 ± 5.7	48 ± 1.1	63 ± 9.0
Inner Diameter, $2a$ (μm)	1161 ± 19.4	1233 ± 38.9	1402 ± 14.7[1,2]	996 ± 14.3[1,2,3]	971 ± 48.1	1123 ± 36.2[3]	1050 ± 18.0[2,3]	1263 ± 36.3	1415 ± 45.5	1199 ± 31.3[b]	1397 ± 42.9[c]
Dimensions at Systolic Pressure P (mmHg)	$P = 120$	$P = 160$	$P = 153$	$P = 121$	$P = 152$	$P = 168$	$P = 107$	$P = 124$	$P = 175$	$P = 117$	$P = 185$
Wall Thickness, h (μm)	38 ± 0.4	58 ± 12.4	41 ± 2.2	54 ± 1.9	54 ± 1.7	51 ± 1.8	49 ± 1.4	42 ± 2.2	58 ± 5.5	44 ± 1.1	61 ± 9.0
Inner Diameter, $2a$ (μm)	1277 ± 28.1	1313 ± 44.1	1535 ± 15.6[1,2]	1057 ± 12.8[1,2,3]	1015 ± 51.6	1188 ± 40.1[3]	1233 ± 25.2[3,4]	1342 ± 37.8	1487 ± 48.0	1307 ± 30.9[b]	1459 ± 45.9
Distensibility (1/MPa)	20.80 ± 1.97	11.47 ± 1.29[1]	16.59 ± 0.48[2]	12.74 ± 0.76[1]	8.11 ± 0.24	8.93 ± 0.49[1,3]	30.37 ± 1.06[1,2,3,4,5]	14.17 ± 0.71	8.03 ± 0.14[a]	19.39 ± 1.19[a,b]	7.55 ± 1.03[a,c]
Additional Metrics at Systolic Pressure											
Circumferential Stretch, λ_θ	1.82 ± 0.04	1.74 ± 0.10	1.98 ± 0.02	1.56 ± 0.04[3]	1.67 ± 0.03	1.64 ± 0.05[3]	1.66 ± 0.03	1.53 ± 0.01	1.63 ± 0.03	1.55 ± 0.04	1.64 ± 0.09
Circumferential Cauchy Stress, σ_θ (kPa)	267 ± 8.4	302 ± 36.8	384 ± 19.3[1]	159 ± 4.9[2,3]	190 ± 3.6	263 ± 13.5[3]	181 ± 7.6[2,3]	269 ± 9.5	304 ± 18.1	230 ± 6.5	340 ± 45.7
Axial Cauchy Stress, σ_z (kPa)	221 ± 7.9	239 ± 30.6	277 ± 13.1	133 ± 9.2[2,3]	152 ± 11.8	178 ± 6.4[3]	171 ± 10.0[3]	220 ± 13.0	215 ± 11.6	192 ± 8.2	223 ± 31.2
Circ. Linearized Material Stiffness, $\mathscr{C}_{\theta\theta\theta\theta}$ (MPa)	1.81 ± 0.09	2.39 ± 0.14	2.51 ± 0.14[1]	1.52 ± 0.06[2,3]	2.11 ± 0.00	2.49 ± 0.09[1,4]	1.15 ± 0.04[2,3,5]	2.26 ± 0.10	3.01 ± 0.15	1.67 ± 0.08	3.74 ± 0.61[c]
Axial Linearized Material Stiffness, $\mathscr{C}_{zzzz}$ (MPa)	3.15 ± 0.35	3.93 ± 0.48	3.95 ± 0.11	2.52 ± 0.41	3.87 ± 0.06	3.25 ± 0.22	2.65 ± 0.19	3.12 ± 0.27	3.43 ± 0.24	2.32 ± 0.19	3.29 ± 0.47
Stored Strain Energy Density, W (kPa)	60 ± 2.7	61 ± 9.5	86 ± 4.3	26 ± 1.5[1,2,3]	27 ± 0.6	41 ± 2.8[3]	39 ± 3.0[3]	57 ± 3.4	54 ± 3.5	51 ± 2.2	61 ± 10.6

Table continues on next page.

Dimensions at Fixed Pressure P (mmHg)	$P = 100$	$P = 100$	$P = 100$	$P = 100$	$P = 100$	$P = 100$	$P = 100$	$P = 100$	$P = 100$	$P = 100$	$P = 100$
Wall Thickness, h (μm)	40 ± 0.4	63 ± 12.4	46 ± 2.5	55 ± 1.9	57 ± 1.9	55 ± 1.7	50 ± 1.4	43 ± 2.3	64 ± 6.0	46 ± 1.1	67 ± 9.2
Inner Diameter, $2a$ (μm)	1220 ± 23.6	1183 ± 36.5	1357 ± 14.6[2]	1025 ± 13.5[1][2][3]	956 ± 46.7	1083 ± 34.0[3]	1211 ± 23.9[3][4]	1289 ± 36.8	1347 ± 43.1	1262 ± 31.0	1299 ± 40.3
Additional Metrics at Fixed Pressure	$P = 100$	$P = 100$	$P = 100$	$P = 100$	$P = 100$	$P = 100$	$P = 100$	$P = 100$	$P = 100$	$P = 100$	$P = 100$
Circumferential Stretch, λ_θ	1.75 ± 0.03	1.58 ± 0.07	1.76 ± 0.02	1.52 ± 0.03	1.58 ± 0.02	1.50 ± 0.04	1.64 ± 0.03	1.47 ± 0.01	1.49 ± 0.03	1.50 ± 0.04	1.46 ± 0.06
Circumferential Cauchy Stress, σ_θ (kPa)	204 ± 5.7	152 ± 17.1[1]	198 ± 10.2	124 ± 3.6[1][3]	112 ± 1.7	131 ± 6.0[1][3]	163 ± 6.7	201 ± 6.7	144 ± 8.3[1]	184 ± 5.1	145 ± 16.7[1]
Axial Cauchy Stress, σ_z (kPa)	189 ± 6.8	160 ± 20.5	172 ± 8.5	114 ± 7.1[1]	106 ± 4.8	108 ± 4.5[1]	162 ± 9.7	189 ± 11.4	149 ± 10.8	169 ± 7.7	142 ± 15.2
Circ. Linearized Material Stiffness, $\mathscr{C}_{\theta\theta\theta\theta}$ (MPa)	1.25 ± 0.06	0.94 ± 0.05[1]	1.00 ± 0.06	1.08 ± 0.05	0.98 ± 0.02	0.94 ± 0.03[1]	1.00 ± 0.03	1.44 ± 0.06	0.97 ± 0.05[1]	1.22 ± 0.06	0.91 ± 0.07[1][3]
Axial Linearized Material Stiffness, $\mathscr{C}_{zzzz}$ (MPa)	2.48 ± 0.27	2.16 ± 0.27	2.18 ± 0.07	2.07 ± 0.32	2.46 ± 0.21	1.69 ± 0.08	2.46 ± 0.17	2.45 ± 0.23	2.02 ± 0.17	1.90 ± 0.17	1.77 ± 0.17
Stored Strain Energy Density, W (kPa)	50 ± 1.9	38 ± 5.8	54 ± 2.8	22 ± 1.2[1][2][3]	19 ± 0.2	25 ± 1.4[1][3]	36 ± 2.8	49 ± 2.8	35 ± 2.2	44 ± 1.8	35 ± 5.3

Values denote mean±standard error. Superscripted numbers and letters in brackets indicate significant differences ($p < 0.05$, Bonferroni post-hoc test following 3-way analysis of variance (ANOVA; left columns) or two-way ANOVA (right columns)), and refer to group numbers. Statistical tests for groups (1) to (7) were run separate from those for groups (a) to (d).

Table S4: Histological quantification of wall constituents of excessively remodeled wild-type L-NAME+Salt-treated mice.

	Abdominal aorta		Thoracic aorta	
	Normal	Excessively remodeled	Normal	Excessively remodeled
Unloaded Cross-sectional Area [mm²]				
Total	0.148 ± 0.001	0.277 ± 0.001[*]	0.279 ± 0.000	0.609 ± 0.021[*]
Media	0.091 ± 0.001	0.171 ± 0.001[*]	0.218 ± 0.001	0.278 ± 0.017[*]
Adventitia	0.057 ± 0.001	0.106 ± 0.001[*]	0.061 ± 0.001	0.330 ± 0.004[*]
Loaded Cross-sectional Area [mm²]				
Total	0.094 ± 0.002	0.213 ± 0.000[*]	0.188 ± 0.001	0.490 ± 0.021[*]
Media	0.058 ± 0.001	0.131 ± 0.001[*]	0.147 ± 0.002	0.224 ± 0.015[*]
Adventitia	0.036 ± 0.002	0.082 ± 0.000[*]	0.041 ± 0.000	0.265 ± 0.006[*]
Wall Percentage [%]				
Media	61.6 ± 0.8	61.7 ± 0.3	78.1 ± 0.4	45.5 ± 1.2[*]
Adventitia	38.4 ± 0.8	38.3 ± 0.3	21.9 ± 0.4	54.5 ± 1.2[*]
Medial area percentages [%]				
Elastin	20.4 ± 3.1	16.3 ± 0.2	22.1 ± 0.7	19.1 ± 0.9[*]
Smooth Muscle	40.0 ± 3.3	53.1 ± 1.0[*]	27.0 ± 1.5	35.7 ± 1.0[*]
Collagen	35.2 ± 1.3	23.4 ± 1.2[*]	44.1 ± 1.9	39.4 ± 0.8[*]
Glycosaminoglycans	4.5 ± 0.6	7.2 ± 0.7[*]	6.9 ± 0.9	5.8 ± 1.0
Adventitial area percentages [%]				
Elastin	0.4 ± 0.1	0.9 ± 0.1[*]	0.6 ± 0.0	0.3 ± 0.0[*]
Smooth Muscle	-	-	-	-
Collagen	99.6 ± 0.1	99.1 ± 0.1[*]	99.4 ± 0.0	99.7 ± 0.0[*]
Glycosaminoglycans	-	-	-	-

Values denote mean±standard error. Asterisks indicate significant differences ($p < 0.05$, Student t-test).

Table S5: Biomechanical metrics for the descending thoracic aorta (DTA) of female mice.

	$Fbln5^{+/+}$ (7)	$Fbln5^{+/+}$ Salt+L-NAME (8)	$Fbln5^{+/+}$ AngII (9)	$Fbln5^{-/-}$ (10)	$Fbln5^{-/-}$ Salt+L-NAME (11)	$Fbln5^{-/-}$ AngII (12)
	$n = 5$	$n = 5$	$n = 5$	$n = 5$	$n = 6$	$n = 5$
Unloaded dimensions						
Wall Thickness, H (µm)	107 ± 5.7	112 ± 3.3	115 ± 3.1	116 ± 6.5	116 ± 5.7	102 ± 4.2
Inner Diameter, $2A$ (µm)	558 ± 17	619 ± 29	636 ± 10	553 ± 26	571 ± 12	601 ± 27
In Vivo **(Loaded) Axial Stretch,** λ_z	1.52 ± 0.02[5][6]	1.48 ± 0.03	1.56 ± 0.02[2][4][5][6]	1.34 ± 0.01[1][3][7][8][9]	1.29 ± 0.02[1][2][3][7][8][9]	1.31 ± 0.03[1][3][7][8][9]
Dimensions at Diastolic Pressure P (mmHg)	$P = 86$	$P = 131$	$P = 125$	$P = 85$	$P = 133$	$P = 112$
Wall Thickness, h (µm)	41 ± 1.7	42 ± 0.9	40 ± 1.0	59 ± 3.4	61 ± 4.2	52 ± 2.8
Inner Diameter, $2a$ (µm)	1096 ± 9.8[2][3]	1277 ± 34.6[4][5][6][7]	1339 ± 30.4[1][4][5][6][7]	913 ± 23.0[1][2][3][5][7][8][9]	965 ± 19.3[1][2][3][5][8][9]	999 ± 10.0[1][2][3][8][9]
Dimensions at Systolic Pressure P (mmHg)	$P = 121$	$P = 171$	$P = 176$	$P = 123$	$P = 174$	$P = 153$
Wall Thickness, h (µm)	38 ± 1.6	40 ± 1.0	37 ± 1.0	57 ± 3.3	59 ± 4.2	50 ± 2.9
Inner Diameter, $2a$ (µm)	1205 ± 14.1[3]	1356 ± 38.2[3][4]	1445 ± 35.6[4][5][6][7]	965 ± 24.5[1][2][3][5][6][7][8][9]	994 ± 22.4[1][2][3][5][6][7][8][9]	1045 ± 10.6[1][2][3][6][8][9]
Distensibility (1/MPa)	21.13 ± 0.95[2][4][5][6]	11.48 ± 1.32[1][6][7]	11.65 ± 0.42[1][6][7]	11.39 ± 0.74[1][6][7]	5.52 ± 0.51[1][2][3][4][6][7][8][9][10]	8.43 ± 0.63[1][3][6][7]
Additional Metrics at Systolic Pressure						
Circumferential Stretch, λ_θ	1.87 ± 0.04	1.92 ± 0.08[4]	1.97 ± 0.05[4]	1.53 ± 0.04[3][8][9]	1.54 ± 0.05[3][7][8][9]	1.57 ± 0.06[3][8][9]
Circumferential Cauchy Stress, σ_θ (kPa)	261 ± 11.2[3]	389 ± 12.5[1][4][5][6][7]	455 ± 20.5[1][2][4][5][6][7]	142 ± 10.3[1][2][3][5][7][8][9]	199 ± 15.2[2][3][8][9]	215 ± 12.5[3][8][9]
Axial Cauchy Stress, σ_z (kPa)	216 ± 5.9	289 ± 9.2[4][5][6]	321 ± 9.5[1][4][5][6][7]	110 ± 13.7[1][2][3][7][8][9]	143 ± 14.3[2][3][8][9]	150 ± 10.7[2][3][8][9]
Circumferential Linearized Material Stiffness, $\mathscr{C}_{\theta\theta\theta\theta}$ (MPa)	1.68 ± 0.09[2][3][5]	2.92 ± 0.15[1][4][6][7]	3.43 ± 0.12[1][2][3][4][5][6][7]	1.49 ± 0.10[2][3][5][8][9]	2.65 ± 0.18[1][4][6][7][9][10]	2.30 ± 0.11[4][6][9][10]
Axial Linearized Material Stiffness, $\mathscr{C}_{zzzz}$ (MPa)	3.02 ± 0.16	4.90 ± 0.19[4][6]	5.21 ± 0.33[1][4][6][7]	2.33 ± 0.44[8][9]	3.43 ± 0.46	3.14 ± 0.34[9]
Stored Strain Energy Density, W (kPa)	59 ± 2.3[4]	80 ± 5.2[4][5][6]	93 ± 5.6[1][2][4][5][6][7]	21 ± 2.3[1][2][3][7][8][9]	25 ± 3.0[1][2][3][7][8][9]	31 ± 3.0[2][3][8][9]
Dimensions at Fixed Pressure P (mmHg)	$P = 100$	$P = 100$	$P = 100$	$P = 100$	$P = 100$	$P = 100$
Wall Thickness, h (µm)	39 ± 1.7	45 ± 0.9	43 ± 1.0	58 ± 3.3	63 ± 4.2	53 ± 2.8
Inner Diameter, $2a$ (µm)	1146 ± 11.5[3]	1185 ± 32.0[3][4]	1255 ± 26.2[4][5]	937 ± 23.6[1][2][3][5][6][7][8][9]	929 ± 15.9[1][2][3][5][6][7][8][9]	980 ± 9.9[1][2][3][6][7][8][9]
Additional Metrics at Fixed Pressure	$P = 100$	$P = 100$	$P = 100$	$P = 100$	$P = 100$	$P = 100$
Circumferential Stretch, λ_θ	1.79 ± 0.04[4][5]	1.69 ± 0.05	1.73 ± 0.03	1.49 ± 0.04[3][7]	1.45 ± 0.04[1][3][7][9]	1.48 ± 0.05[1][3][7]
Circumferential Cauchy Stress, σ_θ (kPa)	196 ± 8.4[4][5]	175 ± 3.5	196 ± 7.5[4][5]	109 ± 7.7[1][3][7][8][9]	101 ± 6.8[1][2][3][6][7][8][9]	124 ± 6.5[1][3][7][9]
Axial Cauchy Stress, σ_z (kPa)	182 ± 4.1[4][5]	181 ± 8.6[4][5]	171 ± 6.7	97 ± 12.3[1][2][3][7][8][9]	99 ± 6.7[1][2][3][7][8][9]	98 ± 7.9[1][2][3][7][8][9]
Circumferential Linearized Material Stiffness, $\mathscr{C}_{\theta\theta\theta\theta}$ (MPa)	1.16 ± 0.06	0.97 ± 0.04[1]	1.04 ± 0.03	1.03 ± 0.06	0.98 ± 0.04[1]	1.01 ± 0.04
Axial Linearized Material Stiffness, $\mathscr{C}_{zzzz}$ (MPa)	2.31 ± 0.11	2.48 ± 0.11	2.34 ± 0.13	1.97 ± 0.38	2.11 ± 0.17	1.78 ± 0.22
Stored Strain Energy Density, W (kPa)	48 ± 1.7[4][5]	47 ± 2.0[4][5]	53 ± 2.8[4][5]	18 ± 1.9[1][2][3][6][7][8][9]	17 ± 1.9[1][2][3][6][7][8][9]	22 ± 1.9[1][2][3][7][8][9]

Values denote mean±standard error. Superscripted numbers in brackets indicate significant differences ($p < 0.05$, Bonferroni post-hoc test following 3-way analysis of variance), and refer to group numbers; groups (1) to (6) are in Table S3.

Table S6: *p*-values for three-way analysis of variance (ANOVA) terms.

	Infrarenal abdominal aorta (IAA)							Descending thoracic aorta (DTA)							*Myh11*^{+/+} and *Myh11*[R247C/R247C] groups (Table S3)		
	Fbln5^{+/+} and *Fbln5*^{-/-} groups (Table S1, S2)							*Fbln5*^{+/+} and *Fbln5*^{-/-} groups (Table S3, S5)									
	induced HT	genotype	sex	induced HT * genotype	induced HT * sex	genotype * sex	induced HT * genotype * sex	induced HT	genotype	sex	induced HT * genotype	induced HT * sex	genotype * sex	induced HT * genotype * sex	induced HT	genotype	induced HT * genotype
Unloaded dimensions																	
Wall Thickness, H (μm)	0.060	0.678	**0.009**	**0.025**	0.787	0.391	0.776	0.427	0.539	0.184	0.084	0.520	0.558	0.714	**0.003**	0.759	0.692
Inner Diameter, $2A$ (μm)	**0.001**	0.790	0.468	0.474	0.661	0.870	0.344	0.052	**0.019**	0.097	0.164	0.645	0.354	0.437	0.606	0.609	0.592
In Vivo (Loaded) Axial Stretch, λ_z	**0.047**	**0.000**	**0.017**	0.677	0.727	0.285	0.365	**0.000**	**0.000**	0.691	**0.045**	0.374	0.093	0.961	0.146	0.914	0.918
Dimensions at Diastolic Pressure																	
Wall Thickness, h (μm)	0.053	**0.000**	0.055	0.077	0.725	0.431	0.820	0.372	**0.009**	0.478	0.648	0.750	0.231	0.563	**0.024**	0.663	0.852
Inner Diameter, $2a$ (μm)	**0.000**	**0.000**	**0.006**	**0.028**	0.669	0.881	0.562	**0.000**	**0.000**	**0.008**	**0.006**	**0.037**	0.230	0.876	**0.000**	0.332	0.573
Dimensions at Systolic Pressure																	
Wall Thickness, h (μm)	**0.028**	**0.000**	0.077	0.116	0.698	0.457	0.794	0.300	**0.006**	0.548	0.654	0.775	0.234	0.552	**0.019**	0.701	0.963
Inner Diameter, $2a$ (μm)	**0.000**	**0.000**	**0.002**	**0.010**	0.743	0.800	0.603	**0.000**	**0.000**	**0.003**	**0.014**	**0.046**	0.275	0.897	**0.002**	0.471	0.938
Distensibility (1/MPa)	**0.000**	**0.000**	**0.005**	0.275	0.197	0.234	**0.045**	**0.000**	**0.000**	**0.026**	**0.024**	0.360	0.963	0.065	**0.000**	**0.029**	**0.010**
Additional Metrics at Systolic Pressure																	
Circumferential Stretch, λ_θ	**0.042**	**0.000**	**0.008**	0.143	0.670	0.731	0.508	0.151	**0.000**	0.970	0.349	0.815	0.074	0.424	0.155	0.857	0.908
Circumferential Cauchy Stress, σ_θ (kPa)	**0.000**	**0.000**	0.061	**0.004**	0.342	**0.036**	0.089	**0.000**	**0.000**	0.260	0.131	0.237	**0.017**	0.265	**0.033**	0.977	0.251
Axial Cauchy Stress, σ_z (kPa)	**0.030**	**0.000**	**0.017**	0.124	0.669	0.120	0.501	**0.000**	**0.000**	0.678	0.376	0.457	**0.034**	0.588	0.565	0.675	0.429
Circumferential Linearized Material Stiffness, $\mathscr{C}_{\theta\theta\theta\theta}$ (MPa)	**0.000**	**0.003**	**0.020**	0.074	0.259	**0.039**	**0.005**	**0.000**	**0.000**	**0.002**	0.161	**0.009**	0.055	**0.004**	**0.003**	0.862	0.127
Axial Linearized Material Stiffness, $\mathscr{C}_{zzzz}$ (MPa)	**0.000**	0.794	0.101	0.084	0.159	0.445	0.225	**0.000**	**0.000**	0.402	0.365	0.389	0.067	0.380	0.092	0.215	0.378
Stored Strain Energy Density, W (kPa)	**0.000**	**0.000**	0.441	**0.044**	0.837	0.382	0.926	**0.000**	**0.000**	0.671	0.139	0.409	0.067	0.590	0.639	0.984	0.392
Dimensions at Fixed Pressure (P=100 mmHg)																	
Wall Thickness, h (μm)	**0.003**	**0.000**	0.095	0.078	0.609	0.480	0.706	0.208	**0.012**	0.554	0.562	0.800	0.262	0.520	**0.005**	0.681	0.993
Inner Diameter, $2a$ (μm)	**0.000**	**0.000**	**0.001**	0.051	0.756	0.700	0.763	**0.000**	**0.000**	**0.000**	0.201	0.099	0.668	0.943	0.241	0.349	0.793
Additional Metrics at Fixed Pressure (P=100 mmHg)																	
Circumferential Stretch, λ_θ	**0.000**	**0.000**	**0.002**	**0.038**	0.477	0.551	0.244	0.273	**0.000**	0.706	0.140	0.867	0.115	0.267	0.827	0.994	0.596
Circumferential Cauchy Stress, σ_θ (kPa)	**0.000**	**0.000**	0.849	**0.000**	0.473	0.404	0.789	**0.004**	**0.000**	0.625	0.306	0.569	0.243	0.626	**0.001**	0.531	0.484
Axial Cauchy Stress, σ_z (kPa)	**0.037**	**0.000**	0.084	0.140	0.817	0.230	0.673	0.571	**0.000**	0.687	0.800	0.609	0.320	0.876	**0.015**	0.289	0.615
Circumferential Linearized Material Stiffness, $\mathscr{C}_{\theta\theta\theta\theta}$ (MPa)	**0.000**	**0.001**	0.546	**0.000**	0.269	0.432	0.911	**0.000**	0.107	0.984	0.103	0.227	0.791	0.849	**0.000**	**0.045**	0.215
Axial Linearized Material Stiffness, $\mathscr{C}_{zzzz}$ (MPa)	0.085	0.679	0.091	**0.013**	0.415	0.352	0.596	0.241	**0.049**	0.903	0.418	0.703	0.509	0.524	0.155	**0.043**	0.429
Stored Strain Energy Density, W (kPa)	**0.002**	**0.000**	0.862	**0.048**	0.927	0.793	0.792	**0.016**	**0.000**	0.734	0.538	0.533	0.235	0.619	**0.010**	0.514	0.601

Statistically significant ($p < 0.05$) values are printed in bold.